

# Self-regulated parallel process 3-D array microfabrication with metal direct-write

Yong Zhang<sup>a,1,\*</sup>, Yen-Po Lin<sup>a,1</sup>, Xianyun Zhang<sup>b</sup>, Yifan Zhang<sup>b</sup>, Jianjun Guo<sup>b,\*</sup>

<sup>a</sup>School of Aerospace Engineering, Georgia Institute of Technology, 270 Ferst Drive, NW, Atlanta, GA 30332, USA

<sup>b</sup>Zhejiang Key Laboratory of Additive Manufacturing Materials, Ningbo Institute of Materials Technology & Engineering, Chinese Academy of Sciences, Ningbo 315201, P. R. China

## ARTICLE INFO

### Article history:

Received 26 February 2021

Revised 18 May 2021

Accepted 29 May 2021

### Keywords:

Meniscus-confined direct-write

Parallel process

Metal microstructures

Electrodeposition

Self-regulating

## ABSTRACT

Parallel process direct-write manufacturing of ultrahigh aspect ratio 3-D metal microstructures remains one of the ultimate challenges in 3-D manufacturing. Its development promises novel solutions for high density chip scale packaging and sorting that require precision microscale mechanical and electrical interfaces to microelectronics. Herein, we exploited a self-regulated growth mechanism revealed in the meniscus-confined direct-write electro-deposition to realize the parallel process fabrication of high-density area arrays of ultrahigh aspect-ratio metal microwire structures. We demonstrated the direct-write fabrication of an array of curvilinear metal spirals over 800  $\mu\text{m}$  in height and 50  $\mu\text{m}$  in array spacing, structurally and mechanically appropriate for high density wafer probe testing applications that cannot otherwise be fabricated with any other existing methods.

© 2021 Elsevier Ltd. All rights reserved.

## 1. Introduction

Ultrahigh aspect-ratio structures with high resolution features are necessary interfaces in advanced system packaging of microchips as well as in integration of microelectronics with multifunctional sensor networks and even biological living systems. Such is the case in the development of 3-D chips with the use of silicon vias in chip scale packaging for multilayer interconnections [1], and in the development of neural probes with high density microneedle arrays for brain stimulation [2]. Besides functioning as conductive paths, such high aspect-ratio 3-D interface structures integrated within these systems need to meet the stringent thermomechanical compatibility requirement in the chip scale packaging application [3], and biocompatibility requirement in the neural probe application [4]. Further on, the fabrication of such precision interfaces should be based on parallel process manufacturing to make the integration of such components in dedicated applications economically viable.

Currently, the common methods for high aspect ratio metal structure microfabrication are surface micromachining based, LIGA (a German acronym for a process involving lithography, electroforming, and moulding) based or 3-D printing based. The surface

micromachining-based method relies on the 2-D photolithography-based processes, which limits its development only for microstructures fewer than 1 mm in feature height [5]. The LIGA based approach makes use of x-ray from a synchrotron for exposure of very thick specialty photoresists to make microstructures up to several millimetres in height [5]. However, it is incompatible with the common photolithography-based microfabrication processes for making microchips. The 3-D printing-based technology is the most versatile and is theoretically not limited to make microstructures of any meaningful height, but is currently not capable of fabricating electronics-quality metal microstructures and is limited to serial process fabrication [6–10]. Towards the ultimate development, an ideal 3-D precision manufacturing technology should be capable of performing scalable parallel process multi-material manufacturing with microscale and even nanoscale resolution, and have the inherent process-compatibility to existing micro-fabrication processes while eliminating the z dimension restriction.

The realization of versatile high-density and high aspect ratio microarrays fabrication would truly stimulate exciting new applications especially in the development of system interfaces that provide mechanical and electrical transitions from microscale to mesoscale, such as in chip scale packaging, in wafer scale testing and in biological cell-electronics integration. The high conductive and elastic 3D helical arrays can also be used as interconnects for wearable electronics, as it can reliably integrated with different components [11]. Furthermore, extending the fabrication methods

\* Corresponding authors.

E-mail addresses: [yong.zhang@ae.gatech.edu](mailto:yong.zhang@ae.gatech.edu) (Y. Zhang), [jiguao@nimte.ac.cn](mailto:jiguao@nimte.ac.cn) (J. Guo).

<sup>1</sup> These authors contributed equally to this work.

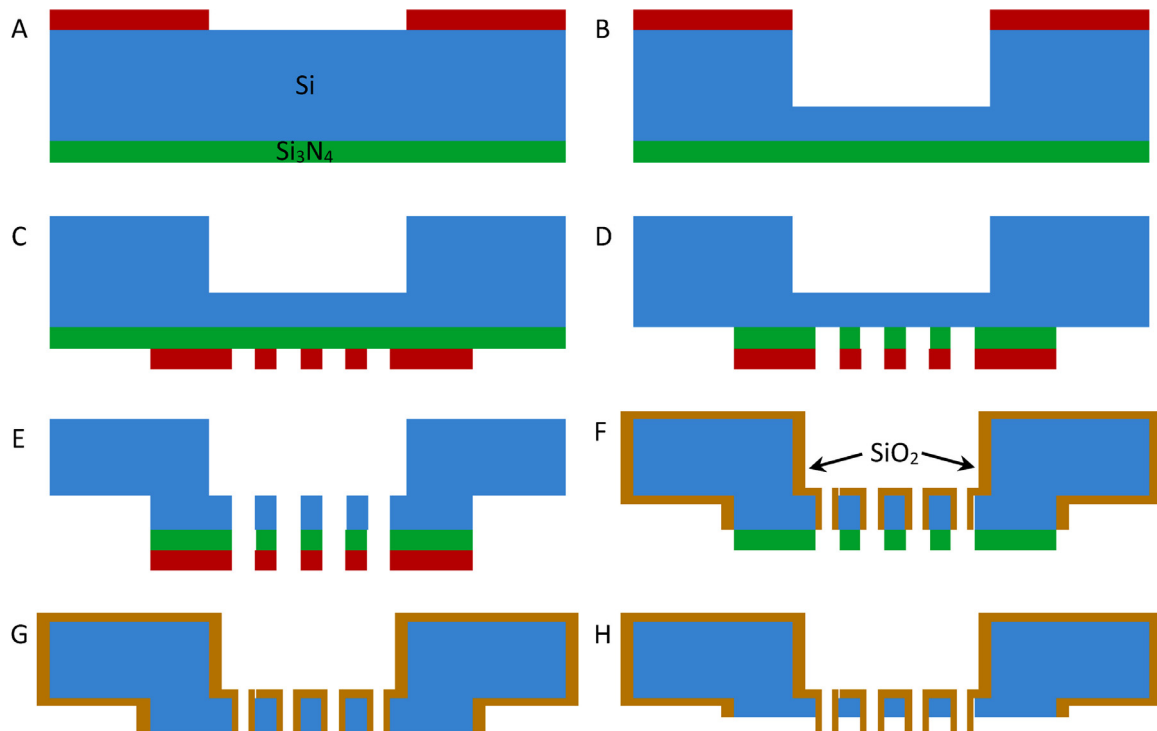


Fig. 1. The fabrication process of a nozzle array.

to other materials and nanocomposites can enables a broad array of applications, including biocompatible 3D cylindrical meshes for stents, high-sensitivity strain sensors, and micro Ka band helical antennas [12]. For microoptics and photonic metamaterial applications, the density of microstructures is also essential, since both the feature size and spacing of individual features must be comparable to the wavelength. [13]

We explore, in this study, a self-regulated growth mechanism revealed in the meniscus- confined direct-write electrodeposition method [14] to realize the parallel process fabrication of high-density area arrays of ultrahigh aspect-ratio metal microwire structures with designed shape and mechanical characteristics.

## 2. Experimental methodology

### 2.1. The surface micromachining process for the fabrication of a nozzle array

The nozzle array fabrication process starts with a double-side polished Si wafer of 480  $\mu\text{m}$  in thickness. As shown in Fig. 1, eight main steps are included: (A) A  $\text{Si}_3\text{N}_4$  film of 100 nm in thickness is deposited onto one side of the wafer via low-pressure chemical vapor deposition. Photoresist is spun and patterned on the other side of the wafer. (B) Deep reactive ion etching (DRIE) is used to etch down 380  $\mu\text{m}$  of silicon from the back side of the Silicon wafer to form cavities as electrolyte reservoirs. (C) Photoresist is spun and patterned on the  $\text{Si}_3\text{N}_4$  side of the wafer to define the circular nozzle shapes. (D) Reactive ion etching (RIE) is used to etch the nitride layer. (E) DRIE is used to etch through the Si membrane to form the nozzle channels. (F) The Si surfaces not covered by  $\text{Si}_3\text{N}_4$  are thermally oxidized to form 1  $\mu\text{m}$  thick  $\text{SiO}_2$ . (G)  $\text{Si}_3\text{N}_4$  is etched off by RIE. (H) DRIE is used to etch down silicon to expose  $\text{SiO}_2$  shells that will serve as the protruding array nozzles for the parallel process direct-write electrodeposition.

### 2.2. Elastic property measurement of the deposited Cu wires

Mechanical characterization of the deposited Cu wires was performed through a cantilever deflection test by a Hysitron Nanoindenter with a flat-ended tip. The indentation was performed at a spot about 20  $\mu\text{m}$  from the free end of the wire. Applying a cantilever stiffness model, the Young's modulus ( $E$ ) was calculated using the following equation:

$$E = \frac{4kl^3}{3\pi r^4}$$

where  $r$  and  $l$  are the diameter and length of the metal wires;  $k$  is the stiffness of wires, which is obtained by the slope of the force vs. deflection curves. The average value of five identical testing results were presented.

The uniaxial compression test with the use of a flat-ended indenter probe was carried out on selected 12 individual spirals similar to that shown in Fig. 4. 75,000 loading-unloading cycles were performed with the dynamic mode of the Nanoindenter. The spiral was compressed to the maximum indentation depth allowed by the available Hysitron Nano-indenter, which is  $\sim 4.5 \mu\text{m}$ , without displaying any plastic deformation behavior. For comparison, straight copper wires were also tested. To avoid non-axial torsion, a short wire having a diameter of  $\sim 30 \mu\text{m}$  and aspect ratio of length to diameter in the range 2.97 to 3.05 was used. Finite element analysis with ANSYS was used to simulate the compression test and to reveal the stress distribution in the wire.

## 3. Theory and calculation

### 3.1. Diffusion zone analysis

In an electrodeposition system where mass transfer process is the rate determining process, deposition rate is mainly governed by the time it took to transport ions to the reaction interface by migration, diffusion and/or convection [15]. Unique to the parallel process nozzle array based electrodeposition method we reported

here, how rapid and uniform ions transport through every individual nozzle channel is critically related to whether or not sustained and uniform deposition under each nozzle can be realized. Two major issues are related to the uniform transport of ions through every nozzle channel during array-based electrodeposition. One is the uniformity of the diffusion zone development [16, 17] over the back openings of the nozzle channels, and the other is the uniformity of evaporation rate around the exposed menisci between every nozzle end and the corresponding growth front of metal wires.

We first discuss the issue of diffusion zone development over nozzle back openings. The close spacing of the nozzle openings at the reservoir side will result in diffusion zone overlap between the neighboring nozzles as the electrodeposition process evolves. For a finite sized nozzle array, however, the diffusion zone development over the peripheral nozzles is different from those over the inner nozzles simply due to the different layout of neighboring nozzles. The diffusion zone development over the peripheral nozzles is allowed to extend further into the bulk electrolyte due to the existence of less numbers of closely-spaced neighboring nozzles. This, in turn, results in higher diffusion limited ion current (thus higher deposition rate) through the peripheral nozzles than that through the inner nozzles, and makes it infeasible to sustain continuous co-growth of metal wires across the whole nozzle array. The problem, however, can be alleviated by the proper design of the nozzles having certain finite channel lengths, effectively converting an inlaid disk electrode array related diffusion problem into a recessed disk electrode array problem, as we analyze below.

The diffusion-limited ionic current through a nozzle in an infinite nozzle array was derived by modifying Wilke's model [17] with the consideration of recessed disk electrode configuration [18] in our system. The following non-dimensionalized equation (the derivation is provided in the later section) generalizes the relationship between the ionic current through each individual nozzle and the relevant geometric dimensions of the nozzle:

$$\frac{1}{i^*} = \left[ 1 + \frac{8}{\pi} AR \right] + \frac{1}{SR^2} \sqrt{\pi t^*} \quad (1)$$

in which the non-dimensionalized ionic current  $i^*$  is defined by  $i/i_{ss}$ , with  $i$  the ionic current through each nozzle and  $i_{ss}$  the steady state ionic current of an inlaid disk electrode having the same diameter as the nozzle opening.  $AR$  is the aspect-ratio of the nozzle,  $SR$  is the ratio of array spacing to nozzle diameter,  $t^*$  is the non-dimensionalized time,  $t^* = Dt/r^2$ ,  $D$  is the diffusion coefficient of metal ion,  $r$  is the radius of the nozzle.

We rely on Eq. (1) to discuss the importance of nozzle design on minimizing the ionic current difference (thus the deposition rate difference) between through peripheral and through inner nozzles in our array-based electrodeposition system. Two geometric variables in this dimensionless equation, the aspect ratio ( $AR$ ) of the nozzle and the array spacing to nozzle diameter ratio ( $SR$ ), are adjusted upon fixing the diameter ( $2r$ ) of the nozzle. In general, increasing the array spacing to nozzle diameter ratio ( $SR$ ) reduces the diffusion zone overlap over neighboring nozzles and also minimizes the difference in diffusion zone development between over the peripheral nozzle and over the inner nozzle. However, increasing the array spacing to nozzle diameter ratio ( $SR$ ) limits the development of high-density metal wire arrays. Increasing the aspect ratio ( $AR$ ) of the nozzle minimizes the diffusion zone overlap over neighboring nozzles but reduces the overall ionic current through the nozzle, thus lowers the overall electrodeposition rate for growing metal wires.

### 3.2. Ionic current analysis

The geometry for the diffusion model consideration of the nozzle array is schematically shown in Fig. 2, where  $L$ ,  $d$ ,  $r$ ,  $\delta$ , are

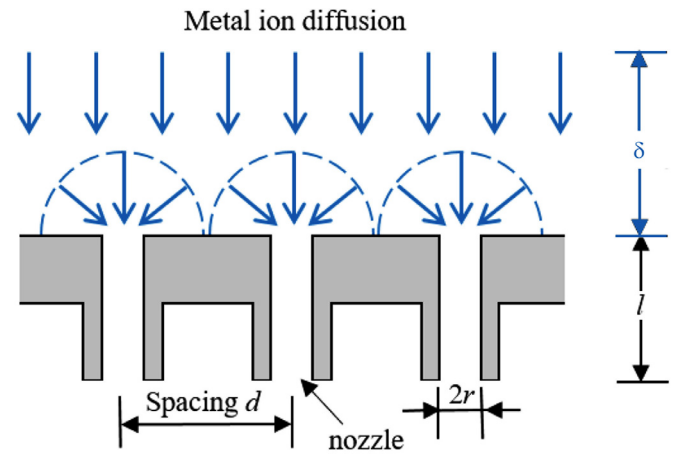


Fig. 2. Schematic showing the geometric layout of a nozzle array and the diffusion zones for the model analysis.

length of the nozzle, array spacing, inner radius of the nozzle, and Nernstian diffusion thickness, respectively. The current through a nozzle array is considered in two serial steps, one involves a planar diffusion from the bulk solution to an imaginary boundary plane, and the other involves a hemispherical diffusion from that imaginary boundary plane to the nozzle opening, as shown in Fig. 2. In the derivation, we excluded the consideration of the effect of convection, and the transition from planar diffusion to hemispherical diffusion at the initial stage of the diffusion field development [15]. The model was thus used to describe the long-term Cottrellian behavior of the chronoamperometric response of a microelectrode array, and to quantitatively predict the electrodeposition rate occurred under each nozzle in our array based direct-write process.

The ion flux across the imaginary boundary plane is:

$$\frac{dn}{dt} = DA(c_b - c_i)/\delta \quad (2)$$

where  $c_b$  and  $c_i$  are the ion concentration in the bulk solution and at the imaginary plane, respectively,  $D$  is the diffusion coefficient of the ion, and  $A$  is the total area of the array.  $\delta$  is the Nernstian diffusion thickness and is defined as  $\delta = \sqrt{\pi dt}$ , which increases with time  $t$ . The ion flux related to the hemispherical diffusion towards the nozzle opening is described by considering the steady state current for recessed disk electrodes. The steady state current for a recession disk can be found in [18]:

$$I_{ss} = zFDrc_i \left( \frac{4\pi r}{\pi r + 4L} \right) \quad (3)$$

where  $z$  is charge number of ion,  $F$  is the Faraday constant,  $r$  is the nozzle diameter,  $L$  is the nozzle length and  $c_i$  is the ion concentration at the imaginary plane.

For a nozzle array with total number of nozzles of  $N$ , the ion flux related to the hemispherical diffusion is then:

$$\frac{dn}{dt} = I/zF = NI_{ss}/zF = NDrc_i \left( \frac{4\pi r}{\pi r + 4L} \right) \quad (4)$$

As the ion flux is continuous through the imaginary boundary, we then have:

$$I = zFDA(c_b - c_i)/\delta \quad (5)$$

The current through each individual nozzle is then obtained by eliminating  $c_i$ :

$$\frac{1}{i} = \frac{1}{zFDrc_b \left( \frac{4\pi r}{\pi r + 4L} \right)} + \frac{N\delta}{zFDAc_b} \quad (6)$$

The equation is non-dimensionalized by normalizing the current with the steady state current of an in-laid disk electrode,  $i_{ss,id}$ :

$$i^* = i/i_{ss,id} = \frac{i}{4zFDrc_b} \quad (7)$$

So

$$\frac{1}{i^*} = \frac{1}{\left(\frac{\pi r}{\pi r + 4L}\right)} + \frac{4N\delta r}{A} \quad (8)$$

For a square  $n \times n$  nozzle array with uniform distribution of nozzles,  $N = n^2$ , and  $A = (n \cdot d)^2$ , so

$$\frac{1}{i^*} = \left(1 + \frac{4L}{\pi r}\right) + \frac{4r\sqrt{\pi Dt}}{d^2} \quad (9)$$

Defining the aspect ratio of nozzle  $AR = L/2r$ , and the array spacing to diameter ratio  $SR = d/2r$ , we have

$$\frac{1}{i^*} = \left(1 + \frac{8}{\pi}AR\right) + \frac{2\sqrt{\pi Dt}}{d} \frac{1}{SR} \quad (10)$$

Further defining a non-dimensional time as  $t^* = \frac{Dt}{r^2}$ , which is also the mass-transfer Fourier number, we have the final form of the following dimensionless equation:

$$\frac{1}{i^*} = \left(1 + \frac{8}{\pi}AR\right) + \sqrt{\pi t^*} \frac{1}{SR^2} \quad (11)$$

The equation contains two parts, one is the time-invariant part in the bracket containing hemispherical diffusion resistance of individual nozzle that depends on nozzle geometry  $AR$ , and the other part is the time-variant part involving the diffusion resistance due to the diffusion zone overlap between neighboring nozzles that depends on the array parameter  $SR$ . When set  $t^* = 0$  and  $AR = 0$ ,  $i = 4zFDrc$  can be obtained, which is the steady state current for an inlaid disk electrode. If we take  $t^* = 0$ ,  $AR$  as an arbitrary number, Eq. (11) reduces to

$$i^* = \frac{\pi r}{\pi r + 4L} \quad \text{or} \quad i = zFDrc \left[ \frac{4\pi r}{\pi r + 4L} \right] \quad (12)$$

which is the steady state current for a recessed disk electrode.

### 3.3. Stability window calculation

Many practical issues exist in a nozzle array-based electrodeposition process that would make it impossible to keep the electrodeposition condition under each nozzle in a nozzle array exactly the same. As we discussed above, the difference in diffusion limited current between through the peripheral nozzles and through the inner nozzles, while can be minimized by design, cannot, theoretically, be eliminated. Issues such as the homogeneity of humidity across the nozzle array, the misalignment between the nozzle array and the substrate surface, and the microfabrication resolution of the nozzle array itself, can all introduce inhomogeneity in electrodeposition conditions across the nozzles in a nozzle array. The self-regulated growth mechanism intrinsic to our meniscus confined electrodeposition method can accommodate, to a certain degree, those practically existing variations, and make it possible to achieve uniform and continuous growth of metal wires across the whole nozzle array.

The thermodynamic consideration of the meniscus at the solid/liquid/air interface dictates the existence of a stable meniscus formation up to a certain meniscus height before rupture [14]:

$$\frac{H_M}{H_W} = \cos \varphi_0 \left( \cosh^{-1} \frac{R_N}{R_W \cos \varphi_0} - \cosh^{-1} \frac{1}{\cos \varphi_0} \right) \quad (13)$$

where  $H_M$  is the height of the meniscus,  $R_W$  is the radius of the wire,  $R_N$  is the radius of the nozzle,  $\varphi_0$  is the slope of the meniscus off the growth direction at the three-phase contact line. The

radius of deposited wire, which is also the Kelvin radius critical for the thermodynamic stability analysis of the meniscus, is regulated by the height of the meniscus. Analysis, confirmed by experimental observation, shows that continuous wire deposition can be sustained as long as the radius of the deposited wire is maintained to be no less than 55% of the nozzle radius, in the case of Cu wire electrodeposition [14]. This is experimentally realized by selecting a nozzle withdrawal speed between a lower bound set by the speed for growing a wire having a diameter equal to the nozzle diameter (when the meniscus height is zero) and an upper bound set by the speed for growing a wire having a diameter equal to 55% of the nozzle diameter (when the meniscus is stretched to its limit to keep thermodynamically stable). This existence of a window of stability in the meniscus confined electrodeposition is critically responsible for realizing the synchronized and continuous co-electrodeposition of an array of metal wires. As long as the variations in nozzle dimension, ionic current and the misalignment of the nozzle array with the substrate across the whole nozzle array are minimized to a certain degree, a common window of stability for array growth exists, albeit a somewhat narrower one as a result of overlapping the windows of stability defined by the conditions under every nozzle. A nozzle array withdrawal speed can thus be chosen within this common window of stability to sustain the continuous co-growth of an array of metal microwires.

## 4. Results and discussion

Fig. 3 describes the general principle of this parallel process direct-write for fabrication of high aspect ratio metal microstructures. An array of nozzles was fabricated with the standard surface micromachining method filled with the selected electrolyte solution for metal electrodeposition. The general procedural processes then include the planar alignment of the nozzle array with a substrate surface, the slow descending of the nozzle array to the substrate surface to establish the liquid contact with the substrate surface by the formation of a meniscus (liquid bridge) under each nozzle, the application of an electric potential to initiate the electro-deposition on the substrate, and the withdrawal of the nozzle array from the substrate at a set speed synchronized with the growth rate of the metal wire beneath each meniscus. Fig. 3C-D show the nozzle array used to perform the parallel process metal direct-write. The nozzle array is silicon based and is composed of a reservoir on the back side fabricated through patterned anisotropic etching and a  $20 \times 20$  array of protruding nozzles with an inner diameter of  $20 \mu\text{m}$  and an array spacing of  $50 \mu\text{m}$  fabricated with patterned deep reactive ion etching. The reservoir is filled with a selected electrolyte solution appropriate for a chosen metal deposition, in this demonstration, a 1 M aqueous  $\text{CuSO}_4$  solution for electrodeposition of solid Cu metal microwires. The array electrodeposition process is performed at room temperature in an ambient environment under a controlled relative humidity of 96%. Two-electrode configuration is used for the electrodeposition with the gold coated substrate as the cathode and a copper wire dipped into the reservoir electrolyte as the anode biased at a potential of 0.2 V. The measured overall ionic current is around 120  $\mu\text{A}$ , and the withdrawal speed of the nozzle array for the continuous metal wire electrodeposition is about 40 nm/s.

A high-density array of ultrahigh aspect-ratio Cu spirals fabricated is showed in Fig. 4. The array was fabricated on a gold coated substrate in a single direct-write process without any post-processing procedures. The motion of the nozzle head is programmed to travel with nanopositioning mechanical stages to produce the curvilinear shape of the metal wires. Each spiral consists of two conical helices starting from a  $50 \mu\text{m}$  tall straight Cu segment (which is also the central axis of the spiral), one outward to a maximum diameter of  $100 \mu\text{m}$  and immediately followed by

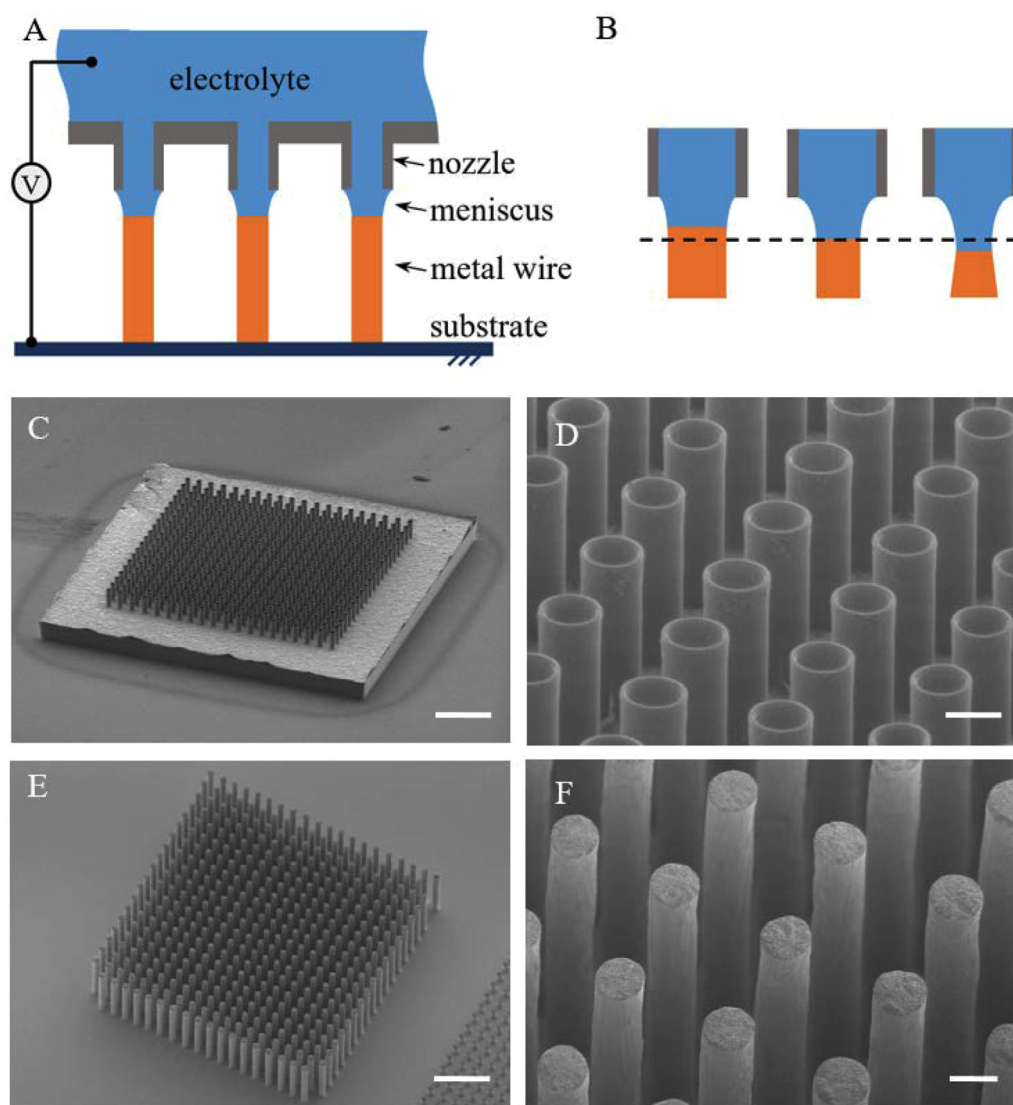


**Fig. 3.** Parallel process direct-write electrodeposition of metal wires. (A) Schematic showing the nozzle array based direct-write electrodeposition within the confined meniscus. (B) Schematic showing stability of the meniscus between the nozzle opening and the wire growth front at various meniscus heights responsible for the self-regulated growth mechanism for sustaining the continuous metal wire growth. Increasing meniscus height leads to smaller diameter (but faster rate) wire growth, then to tapered wire growth and eventually to the breaking of the meniscus. (C) SEM image showing a microfabricated  $20 \times 20$  nozzle array. The scale bar is  $200 \mu\text{m}$ . (D) Close-up SEM image of the nozzle openings. The scale bar is  $20 \mu\text{m}$ . (E) SEM image of a  $20 \times 20$  array of straight Cu microwires grown by the nozzle array with the parallel process direct-write electrodeposition. The scale bar is  $200 \mu\text{m}$ . (F) Close-up SEM image of the Cu wire array. The scale bar is  $20 \mu\text{m}$ .

the other inward helix, both at a cone angle of  $25^\circ$ . The spiral terminates at the geometric center of the spiral with another  $30 \mu\text{m}$  tall straight segment along the central axis. The total height of the spiral is  $805 \mu\text{m}$  and the diameter of the wire is around  $18 \mu\text{m}$ . This array of Cu spirals has a pitch of  $50 \mu\text{m}$ , mirroring exactly the nozzle spacing of the 2-D nozzle array. Further increase of the area density of the spirals is possible with the use of a higher density nozzle array. Further increase of the aspect-ratio of the spirals can be simply realized by continuing the growth process.

Such an array consisting of conductive metal spirals is fabricated following the mechanical and dimensional design requirements potentially appropriate for their applications as wafer probes for chip testing or mechanically compliant interconnects for chip scale packaging. [19, 20] The state-of-the-art compliant interconnects and test probes are typically fabricated with micromachining processes. Due to the intrinsically planar nature of the micromachining processes, the fabrication must consider a difficult trade-off among structural density, aspect ratio, mechanical

performance and process complexity. The parallel process direct-write method overcomes many technical limitations in the existing methods and enables the fabrication of such mechanically ideal, 3-D curvilinear shaped metal microstructure array in a single step.

We characterize the mechanical properties of the fabricated metal microstructure in terms of its elasticity and yielding behavior. From the measured stiffness values shown in Fig. 5, the electrodeposited Cu wires were found to have a Young's modulus of  $121.0 \pm 2.8 \text{ GPa}$ , comparable to that of bulk Cu, because the elastic properties are mostly independent of the microstructure [21]. However, the uniaxial compression yield strength of straight microwires is much larger than that of the bulk copper ( $70\text{--}90 \text{ MPa}$ ), [23] reached  $675 \pm 34.2 \text{ MPa}$ , which is consistent with the literature reports value of  $630\text{--}962 \text{ MPa}$  [21]. This high yield strength is attainable in nanocrystalline Cu due to the Hall-Petch strengthening effect or in nanotwinned Cu, [22, 24–27] and in our case, due to the nano-crystalline structure formation in Cu wire electrodeposited at high diffusion limited current density of near 12

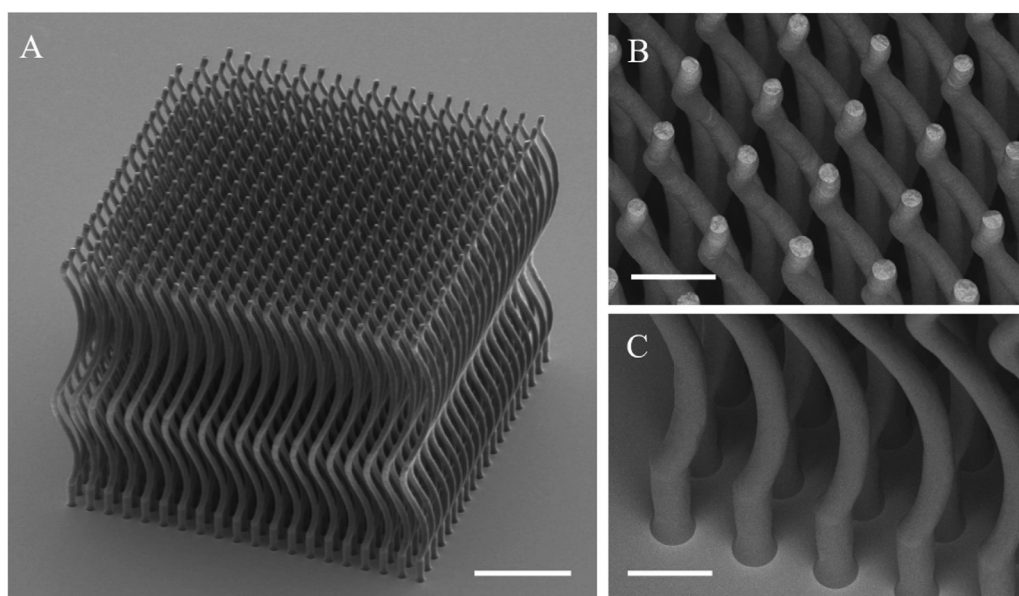


**Fig. 4.** SEM images of a  $20 \times 20$  array of curvilinear Cu spirals fabricated with the parallel process direct-write electrodeposition. (A) Overall view of the array of spirals  $\sim 800 \mu\text{m}$  in height and  $\sim 20 \mu\text{m}$  in wire diameter. The array spacing is  $50 \mu\text{m}$ . The scale bar is  $200 \mu\text{m}$ . (B) Close-up SEM image showing the end segment quality of the Cu spiral array. The scale bar is  $50 \mu\text{m}$ . (C) Close-up SEM image showing the quality of the bases of the Cu spirals. The scale bar is  $50 \mu\text{m}$ .

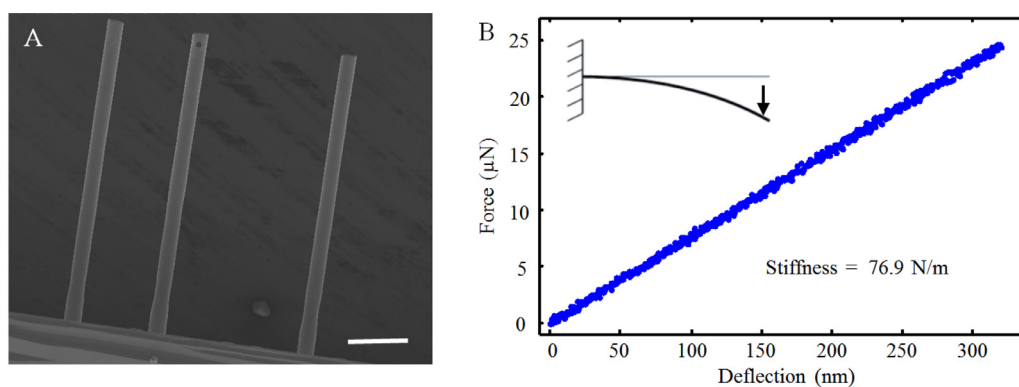


**Fig. 5.** Elastic property measurement of the deposited Cu wires. (A) SEM image showing three straight Cu wires deposited onto a flat substrate. The left wire has a diameter of  $27.0 \mu\text{m}$  and a length of  $511.9 \mu\text{m}$ . The middle wire has a diameter of  $27.0 \mu\text{m}$  and a length of  $510.0 \mu\text{m}$ . The right wire has a diameter of  $26.8 \mu\text{m}$  and a length of  $511.3 \mu\text{m}$ . The scale bar is  $100 \mu\text{m}$ . (B) A representative force vs. deflection curve acquired from the right wire, yielding a stiffness value of  $76.9 \text{ N/m}$ .

$\text{A dm}^{-2}$ . The uniaxial compression results of spirals are shown in Fig. 6. The highest von Mises stress of  $302 \text{ MPa}$  was found to occur at the middle portion of the spiral, however it still much lower than the yield strength of the materials. Fig. 6b shows the shear stress distribution of the spiral tested. The observed uniform stress distribution without obvious stress concentration indicates there is no localized yielding, presumably because of continuous structural shape that has no sharp corner. At the spiral-substrate interface, the majority area of the base of the spiral was subjected to near zero shear stress with the highest shear stress of merely  $2.5 \text{ MPa}$  shown near the edge of the base, a feature potentially beneficial for mitigating the risk of debonding of the spiral from the substrate in real applications. Considering this aspect, the stresses of the copper spiral is much lower than that of the straight line, which exceeds the yielding stress of the copper materials at an identical compression depth of  $4.5 \mu\text{m}$  (Figure S6). To acquire the yield strength of the electrodeposited Cu structure, we performed a displacement controlled cyclic uniaxial compression test on the fabricated Cu spirals with a custom-made mechanical testing setup. The spiral was shown to mechanically yield at a compression of exceeding  $12 \mu\text{m}$ , resulting in a yield strength of almost  $850 \text{ MPa}$  according to the corresponding finite element

analysis. Thus, the observed high von Mises stress of the helix, as compared to the straight wire, is most likely originate from the geometry of the spirals.

The electrical conductivities of the straight and spiral lines, measured by two-electrode mode at standard room temperature and atmospheric pressure, are  $1.74 \times 10^7 \text{ S/m}$  and  $2.12 \times 10^7 \text{ S/m}$ , respectively, comparable to the electrical resistivity of bulk Cu ( $5.71 \times 10^7 \text{ S/m}$ ). This high density high aspect-ratio Cu spiral microstructure array, possessing extremely high mechanical yield strength, intrinsically high electrical conductivity (almost 5 time higher than Ni based material typically used in wafer probe applications) and designed mechanical compliance, could be the ideal interface structure for serving as interconnect in chip scale packaging to alleviate thermomechanical mismatch issues in flip chip bonding, or as wafer testing array probe meeting both mechanical and area density requirements in advanced chip testing.

To be able to successfully produce such 3-D spiral metal microstructure arrays in the described “simple” parallel direct-write process requires, however, exploiting two principle mechanisms intrinsically existed in this fabrication system. One related to the mechanical stability of the meniscus at the interface of the nozzle end opening and the growth front of the metal wire, and the other re-

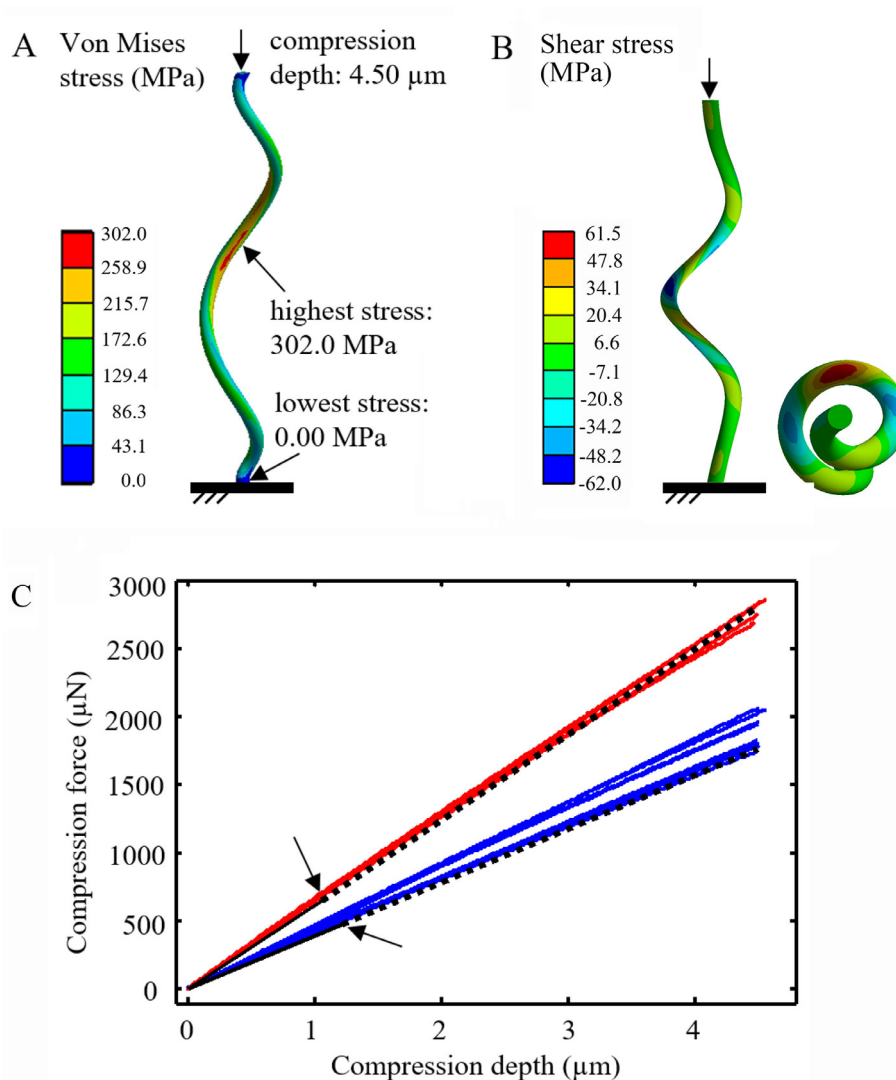


**Fig. 6.** Mechanical characterization of the Cu spirals. (A) Finite element analysis showing the von Mises stress and (B) shear stress distribution in a Cu spiral of having the same overall dimensions as the fabricated spirals and having a wire diameter of 18.5  $\mu\text{m}$  at a compression displacement of 4.5  $\mu\text{m}$ . (C) The compressive load- displacement curves (blue and red lines) acquired from 12 Cu spirals having slightly varying wire diameters from 16.5  $\mu\text{m}$  to 18.5  $\mu\text{m}$  and their comparison with simulation results without considering plastic yielding (black lines, the upper one for a wire having a diameter of 18.5  $\mu\text{m}$  and the lower one 16.5  $\mu\text{m}$ ). The arrows indicate the points when the maximum stress in the wire reaches 80 MPa, the typical yielding strength of bulk copper.

lated to managing the ion diffusion zone overlapping due to the use of a high-density nozzle array involved in electrodeposition. Due to the existence of minute variations in dimensions and surface properties among an array of microfabricated nozzles and the technical difficulty in achieving the perfect parallel alignment between the area nozzle array and the substrate plane, to realize the synchronized and continuous co-growth of an array of metal wire structures without individually-addressable nozzle controls during the whole electrodeposition process requires the involvement of a self-regulated electrodeposition mechanism intrinsically existed in the meniscus confined electro-deposition [14].

The self-regulated growth mechanism in the meniscus confined electrodeposition originates from the thermodynamic stability of liquid meniscus formed between the nozzle end opening and the growth front of the metal wire. The thermodynamic consideration of the meniscus at the solid/liquid /air interface dictates the existence of a stable meniscus formation up to a certain meniscus height before rupture [14]. The radius of deposited wire, which is also the Kelvin radius critical for the thermodynamic stability analysis of the meniscus, is regulated by the height of the meniscus.

Analysis, confirmed by experimental observation, shows that continuous wire deposition can be sustained as long as the radius of the deposited wire is maintained to be no less than 55% of the nozzle radius, in the case of Cu wire electrodeposition. This is experimentally realized by selecting a nozzle withdrawal speed between a lower bound set by the speed for growing a wire having a diameter equal to the nozzle diameter and an upper bound set by the speed for growing a wire having a diameter equal to 55% of the nozzle diameter. This existence of a window of stability in the meniscus confined electrodeposition is essential for realizing the synchronized and continuous co- electrodeposition of an array of metal wires. As long as the variation in nozzle dimension, ionic current and the misalignment of the nozzle array with the substrate are within technically acceptable limit, a common window of stability exists, albeit a somewhat narrower one as a result of overlapping the windows of stability defined by the conditions under every nozzle (Fig. S1 and S2 in Supplement materials). A nozzle array withdrawal speed can thus be chosen within this common window of stability to sustain the continuous co-growth of an array of metal microwires. Such an existence of self-regulation is an

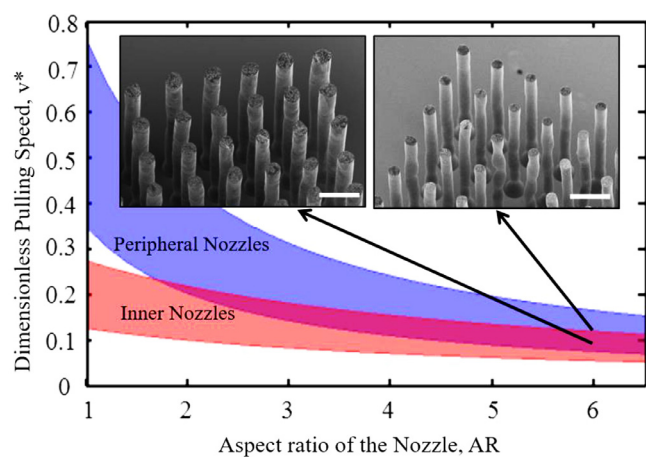


**Fig. 7.** Plot showing the windows of stability for sustaining the continuous wire growth for peripheral nozzles and for inner nozzles, and their dependence on the aspect ratio of the nozzle. The common window of stability for realizing the continuous co-growth of metal wires from every nozzle in the nozzle array occurs in the indicated overlapped region.

intrinsic feature of this meniscus confined electrodeposition, and is not available in any other existing direct-write fabrication methods [6].

Unique to the nozzle array based direct-write electrodeposition, the diffusion zone development over the back openings of nozzle (also termed as electrodes in the nomenclature of electrochemistry) towards the reservoir electrolyte regulates the diffusion limited current through corresponding nozzles [27] and thus the available deposition rate of metal wire under each nozzle. For a uniform nozzle array, the difference in diffusion zone development occurs most pronounced between the peripheral nozzle openings and the inner nozzle openings: the peripheral nozzle has less neighboring nozzles and allows more diffusion zone development into the bulk electrolyte [28]. Biased at the same electrical potential for the electrodeposition, the metal wire growth under the peripheral nozzles can potentially be faster than that under the inner nozzles, or in other words, a common window of stability for electrodeposition for the whole array nozzles may not exist and the continuous co-growth of array wires may not be possible.

The modelled results of the diffusion-limited current through the peripheral nozzle [28] is assumed to be not affected by the neighboring nozzles and remains constant approximately at the onset current defined by the first term in Eq. (1). Accordingly, the difference in the current through the peripheral nozzle and through the inner nozzle can be minimized by increasing the nozzle spacing to diameter ratio SR or the nozzle aspect ratio AR. However, increasing SR compromises the capability of fabricating high-density metal microwire array with this parallel process direct-write approach; increasing AR lowers the diffusion limited current for electrodeposition [18], thus the deposition rate for the co-growth of metal microwires.

Fig. 7 shows the dependence of the window of stability in terms of the nozzle withdrawal speed on the nozzle aspect ratio for the inner nozzle and the peripheral nozzle having a nozzle spacing-to-diameter ratio of 2. The diameter of the nozzle in the modeling is set to be 20  $\mu\text{m}$ . The window of stability for the withdrawal speed for sustaining continuous metal wire electro-deposition is defined according to the previously described criteria developed from the thermodynamic consideration of meniscus stability [14]. The windows of stability as a function of the nozzle aspect ratio are presented for the peripheral nozzle and the inner nozzle in the plot, respectively. As seen, the windows of stability begin to overlap above a nozzle aspect ratio of 2. However, at this low aspect

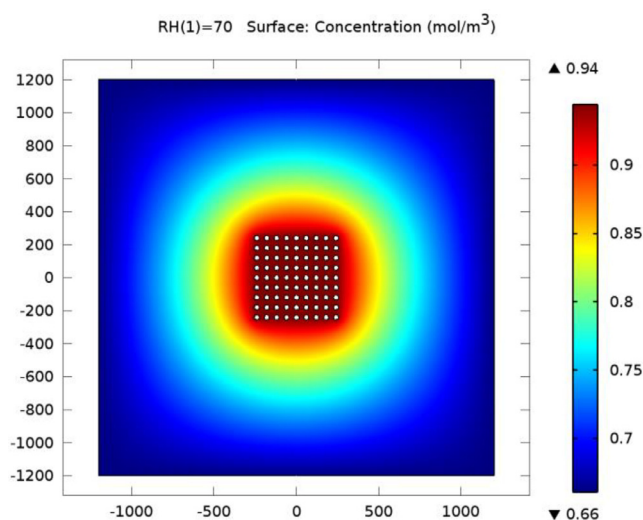


**Fig. 8.** Relative humidity distribution over a  $9 \times 9$  array of nozzle opening filled with water when the surrounding relative humidity is at 70%, simulated with a 2-D diffusion model. The nozzle array has array spacing to diameter ratio (SR) of 2.

ratio, the meniscus under the peripheral nozzle is stabilized for growing metal microwire having a radius close to  $R_N$ , while the inner nozzle for metal microwire having a radius close of  $0.55 R_N$ . A slight deviation from this withdrawal speed from this narrow overlapped zone of window of stability would either cause the clogging in the peripheral nozzle due to the over-growth of the metal wire into the nozzle or the abrupt rupture of meniscus under the inner nozzle due to the overstretching of the meniscus formed between the nozzle and the growth front of the metal wire. Optimal nozzle aspect ratio was found to be at around 6, which provided an overlapped zone of window of stability wide enough to make it technically feasible to realize the simultaneous growth of an array of metal microwires, while in the meantime, minimizing the variation in wire diameters across the whole array and achieving a reasonable growth rate for high throughput fabrication.

Another variable that may affect the uniformity and even feasibility of this parallel process microfabrication is the local humidity around the nozzle head. Different from the conventional electroplating process, which is typically performed inside an electrolyte bath, the existence of a solid/liquid/air interface in our meniscus confined direct-write electrodeposition, while provided the aforementioned unique benefits, would inevitably subject the electrodeposition of metal to the influence of temperature and humidity conditions surrounding the liquid bridges (menisci) established under every nozzle due to the constant occurrence of water evaporation off the menisci. The existence of a humidity gradient across the nozzle array during the electrodeposition process regulates the rate of water evaporation, individually establishes electrolyte conditions in the menisci and thus alters the conditions for the existence of a common window of stability for the co-growth of metal wires across the whole array. Our numerical simulation based on considering the 2-D diffusion of water molecules across the nozzle array in an ambient environment using COMSOL indicates that the water vapor concentration becomes largely homogeneous towards the center beyond the first two or three rows of peripheral nozzles, as shown in Fig. 8, with the line plot showing the relative humidity distribution across the middle row in Fig. S4 and S5. In our experiment, a relative humidity of around 96% was created around the nozzle array to minimize the evaporation from the menisci, achieving a less than 1% difference in evaporation rates from the menisci under all nozzles according to the model analysis.

## 5. Conclusions

The scale up of the meniscus confined 3-D electrodeposition process into a parallel process direct-write for fabricating precision metal microstructure arrays provides a cost effective and flexible method for developing electrical interconnections possessing designed mechanical, thermal and structural properties. Being a direct-write method and thus readily process-compatible with the microfabrication processes for integrated circuits, micro-electro-mechanical systems, microfluidic systems and even micro- opto-electro-mechanical systems can also facilitate cost effective cross-platform integrations of such microsystems and/or enable the incorporation of value-added functions into such microsystems.

## Author statement

**Yong Zhang:** Conceptualization, Methodology, Software, Writing - Original Draft. **Yen-Po Lin:** Conceptualization, Methodology. **Yifan Zhang:** Formal analysis. **Xianyun Zhang:** Software, Data Curation. **Jianjun Guo:** Writing - Review & Editing.

## Author contributions

Yong Zhang and Yen-Po Lin conceived the concept, carried out the experimental sections and wrote the manuscript. Yifan Zhang and Xianyun Zhang Performed part of the modeling. Jianjun Guo reviewed the manuscript. All the authors discussed the results and contributed to the manuscript.

## Declaration of Competing Interest

The authors declare that they have no known competing financial interests or personal relationships that could have appeared to influence the work reported in this paper.

## Supplementary materials

Supplementary material associated with this article can be found, in the online version, at doi:[10.1016/j.apmt.2021.101085](https://doi.org/10.1016/j.apmt.2021.101085).

## References

- [1] J.H. Lau, *Through-Silicon Vias for 3D Integration*, McGraw Hill Professional, New York, 2012.
- [2] M. Delgado-Restituto, A. Rodríguez-Pérez, *Neural recording interfaces for intracortical implants*, in: S. Bhunia, S. Majerus, M. Sawan (Eds.), *Implantable Biomedical Microsystems: Design Principles and Applications*, Elsevier, Kidlington, 2015, pp. 251–279.
- [3] X. Liu, Q. Chen, V. Sundaram, M. Simmons-Matthews, K.P. Wachtler, R.R. Tumala, S.K. Sitaraman, Thermo-mechanical behavior of through silicon vias in a 3D integrated package with inter-chip microbumps, in: 2011 IEEE 61st Electronic Components and Technology Conference (ECTC), 2011, pp. 1190–1195, doi:[10.1109/ectc.2011.5898661](https://doi.org/10.1109/ectc.2011.5898661).
- [4] C. Marin, E. Fernández, Biocompatibility of intracortical microelectrodes: current status and future prospects, *Front. Neuroeng.* 3 (2010) 1–6, doi:[10.3389/fneng.2010.00008](https://doi.org/10.3389/fneng.2010.00008).
- [5] M.J. Madou, *Fundamentals of Microfabrication: the Science of Miniaturization*, 2nd Ed., CRC, Boca Raton, 2002.
- [6] R.D. Farahani, K. Chizari, D. Therriault, Three-dimensional printing of freeform helical microstructures: a review, *Nanoscale* 6 (2014) 10470–10485, doi:[10.1039/c4nr02041c](https://doi.org/10.1039/c4nr02041c).
- [7] S. Reyntjens, R. Puers, A review of focused ion beam applications in microsystem technology, *J. Micromech. Microeng.* 11 (2001) 287–300, doi:[10.1088/0960-1317/11/4/301](https://doi.org/10.1088/0960-1317/11/4/301).
- [8] L.L. Lebel, B. Aissa, M.A. El Khakani, D. Therriault, Ultraviolet-assisted direct-write fabrication of carbon nanotube/polymer nanocomposite microcoils, *Adv. Mater.* 22 (2010) 592–596, doi:[10.1002/adma.200902192](https://doi.org/10.1002/adma.200902192).
- [9] S.Z. Guo, F. Gosselin, N. Guerin, A.M. Lanouette, M.C. Heuzey, D. Therriault, Solvent-cast three-dimensional printing of multifunctional microsystems, *Small* 9 (2013) 4118–4122, doi:[10.1002/sml.201300975](https://doi.org/10.1002/sml.201300975).
- [10] J.J. Adams, E.B. Duoss, T.F. Malkowski, M.J. Motala, B.Y. Ahn, R.G. Nuzzo, J.T. Bernhard, J.A. Lewis, Conformal printing of electrically small antennas on three-dimensional surfaces, *Adv. Mater.* 23 (2011) 1335–1340, doi:[10.1002/adma.201003734](https://doi.org/10.1002/adma.201003734).
- [11] Z. Yang, Z. Zhai, Z. Song, Y. Wu, J. Liang, Y. Shan, J. Zheng, H. Liang, H. Jiang, Conductive and elastic 3D helical fibers for use in washable and wearable electronics, *Adv. Mater.* 32 (2020) 1907495, doi:[10.1002/adma.201907495](https://doi.org/10.1002/adma.201907495).
- [12] L. Liu, L. Zhang, S.Min Kim, S. Park, Helical metallic micro- and nanostructures: fabrication and application, *Nanoscale* 6 (2014) 9355.
- [13] J.K. Gansel, M. Thiel, M.S. Rill, M. Decker, K. Bade, V. Saile, G. von Freymann, S. Linden, M. Wegener, Gold helix photonic metamaterial as broadband circular polarizer, *Science* 325 (2009) 1513.
- [14] J. Hu, M.-F. Yu, Meniscus-confined three-dimensional electrodeposition for direct writing of wire bonds, *Science* 329 (2010) 313–316, doi:[10.1126/science.1190496](https://doi.org/10.1126/science.1190496).
- [15] A.J. Bard, L.R. Faulkner, *Electrochemical methods: Fundamentals and Applications*, 2nd ed., John Wiley & Sons, Danvers, 2001.
- [16] B.R. Scharifker, Diffusion to Ensembles of Microelectrodes, *J. Electroanal. Chem.* 240 (1988) 61–76, doi:[10.1016/0022-0728\(88\)80313-9](https://doi.org/10.1016/0022-0728(88)80313-9).
- [17] S. Wilke, M.D. Osborne, H.H. Girault, Electrochemical characterisation of liquid vertical bar liquid microinterface arrays, *J. Electroanal. Chem.* 436 (1997) 53–64, doi:[10.1016/S0022-0728\(97\)00323-9](https://doi.org/10.1016/S0022-0728(97)00323-9).
- [18] A.M. Bond, D. Luscombe, K.B. Oldham, C.G. Zoski, A comparison of the chronoamperometric response at inlaid and recessed disc microelectrodes, *J. Electroanal. Chem. Interfacial. Electrochem.* 249 (1988) 1–14 [https://doi.org/10.1016/0022-0728\(88\)80345-0](https://doi.org/10.1016/0022-0728(88)80345-0).
- [19] M. Losey, A low-force MEMS probe solution for fine-pitch 3D SiC wafer test, *IEEE International Workshop on Testing Three-Dimensional Stacked Integrated Circuits (3D-TEST)*, 2011.
- [20] K. Kacker, Design and Fabrication of Free-Standing Structures As Off-Chip Interconnects For Microsystems packaging, G. W. Woodruff School of Mechanical Engineering, Georgia Institute of Technology, Atlanta, 2008.
- [21] A. Reiser, L. Koch, K.A. Dunn, T. Matsuura, F. Iwata, O. Fogel, Z. Kotler, N. Zhou, K. Charipar, A. Piqué, P. Rohner, D. Poulidakos, S. Lee, S.K. Seol, I. Utke, C. van Nesselroy, T. Zambelli, J.M. Wheeler, R. Spolenak, Metals by micro-scale additive manufacturing: comparison of microstructure and mechanical properties, *Adv. Funct. Mater.* 30 (28) (2020) 1910491, doi:[10.1002/adfm.201910491](https://doi.org/10.1002/adfm.201910491).
- [22] S. Daryadel, A. Behroozfar, S.R. Morsali, S. Moreno, M. Baniasadi, J. Bykova, R.A. Bernal, M. Minary-Jolandan, Localized pulsed electrodeposition process for three-dimensional printing of nanotwinned metallic nanostructures, *Nano Lett.* 18 (2018) 208–214, doi:[10.1021/acs.nanolett.7b03930](https://doi.org/10.1021/acs.nanolett.7b03930).
- [23] A.M. Howatson, P.G. Lund, J.D. Todd, *Engineering Tables and Data*, Chapman and Hall, London, 1972.
- [24] V.Y. Gertsman, M. Hoffmann, H. Gleiter, R. Birringer, The study of grain size dependence of yield stress of copper for a wide grain size range, *Acta Metall.* 42 (1994) 3539–3544, doi:[10.1016/0956-7151\(94\)90486-3](https://doi.org/10.1016/0956-7151(94)90486-3).
- [25] J. Schiøtz, K.W. Jacobsen, A maximum in the strength of nanocrystalline copper, *Science* 301 (2003) 1357–1359, doi:[10.1126/science.1086636](https://doi.org/10.1126/science.1086636).
- [26] L. Lu, X. Chen, X. Huang, K. Lu, Revealing the maximum strength in nanotwinned copper, *Science* 323 (2009) 607, doi:[10.1126/science.1167641](https://doi.org/10.1126/science.1167641).
- [27] J. Strutwolf, M.D. Scanlon, D.W. Arrigan, Electrochemical ion transfer across liquid/liquid interfaces confined within solid-state micropore arrays—simulations and experiments, *Analyst* 134 (2009) 148–158, doi:[10.1039/b815256j](https://doi.org/10.1039/b815256j).
- [28] S. Wilke, M.D. Osborne, H.H. Girault, Electrochemical characterisation of liquid/liquid microinterface arrays, *J. Electroanal. Chem.* 436 (1997) 53–64 [https://doi.org/10.1016/S0022-0728\(97\)00323-9](https://doi.org/10.1016/S0022-0728(97)00323-9).